Stability of Ground Effect Machines

David I. G. Jones* and Margaret Blake†
Vickers–Armstrongs (South Marston) Ltd., Swindon, England

A theory of the behavior of three-dimensional peripheral jet ground effect machines (GEM's) in pitch and roll is presented. The physical basis of the theory is the satisfaction of continuity of mass flow through the cushion of high-pressure air supporting the craft, and generated by the peripheral jets. Detailed calculations have been carried out for a rectangular craft with a length-to-breadth ratio of two. Comparisons with experimental data are encouraging, although none of the experimental craft were of identical geometry. The assumptions on which the theory is based are discussed, and a need is shown for fundamental experimental work on the behavior of jets.

Nomenclature

A = aspect ratio (length/breadth for pitch)
b = fraction of mass flow to enter cushion from splitting peripheral jet element
f_i = p_i/H
$f(\xi_i), f(\xi)$ = Appendix A and text
$g(\xi_i), g(\xi)$ = Appendix A and text
G_i = $m_i/S_it(\rho H)^{1/2}$ ($= G_{i+} + G_{i-}$)
G_{i+} = positive part of G_i
G_{i-} = negative part of G_i
h = hoverheight at reference point (also hoverheight in general)
$h(\eta_i)$ = hoverheight at station η_i
$h_e(\eta_i)$ = effective hoverheight at station η_i (theory)
H = total head of jets at nozzle exits
i = suffix referring to compartment (i = 1 for compartment tilted towards ground)
I = $\int_0^1 \chi_i d\eta_i$ (theory)
I_+, I_- = positive and negative parts of I, respectively
k = factor describing loss of velocity of jets due to splitting (Appendix B)
L = lift (also suffix referring to longitudinal direction)
l_i = length of longitudinal stability jet in ith compartment (Fig. 1)
l_T = length of transverse stability jet
l = length of craft cushion
M = nose-up restoring couple
m = mass flow rate in general
m_i = net mass flow leaving ith compartment under peripheral jets
m_{pi} = net mass flow out of peripheral nozzle of ith compartment
m_{si} = mass flow through longitudinal stability nozzle in ith compartment.
m_{s3} = net mass flow through transverse stability nozzle
m_{s3i} = fraction of mass flow from transverse stability jet which enters ith compartment
N = percentage shift of center of pressure, based on length of cushion l
p = cushion pressure in general (also suffix to denote periphery)
p_i = cushion pressure in ith compartment
S_i = length of peripheral nozzle in ith compartment
S = nozzle length in general
t = peripheral jet thickness at reference point $\eta_i = 0$ (also jet thickness in general)
$t(\eta_i)$ = peripheral nozzle thickness at station η_i
t_T = thickness of transverse stability nozzle
t_L = thickness of longitudinal stability nozzle
T = suffix referring to transverse
V = velocity in peripheral jet nozzle (also velocity in general)
V_0 = velocity of air leaving cushion under peripheral jet at station η_i
V_c = mean velocity of crossflow in cushion
V_s = velocity of air in stability nozzles
V_1 = velocity of air in compartment 1 prior to underfeeding transverse stability jet (Fig. 6)
V_2 = velocity of air underfeeding transverse stability jet (Fig. 6)
X = $\alpha/\alpha_{\max}$
x = $h/t(1 + \cos\theta)$
$x(\eta_i)$ = $h(\eta_i)/t(1 + \cos\theta)$
y_i = distance around periphery from reference point
α = angle of pitch (or roll) in degrees
$\alpha_{\max}$ = maximum angle of pitch or roll ($2h/l$ rad for pitch)
$\gamma(x)$ = nondimensional mass flow parameter
δh = underfeed height for transverse stability jet
$\delta h(\eta_i)$ = underfeed height for peripheral jet at station η_i
δH = head rise across fan(s)
δm_i = mass flow leaving cushion under element y_i of peripheral jet at station η_i
$\delta m(\eta_i)$ = mass flow through element δy_i of peripheral nozzle at station η_i
δm_c = crossflow
η_i = Y_i/S_i fractional distance around periphery of ith compartment
θ = peripheral jet angle relative to horizontal on low pressure side of jet
μ = factor describing loss of momentum in crossflow (Eq. 4)
ν = kinematic viscosity of air
ξ = effective value of x for transverse stability jet
ξ_i = effective value of x for peripheral jet in ith compartment
ρ = density of air
σ = N/α, pitch or roll stiffness based on length l expressed as a percentage shift of the center of pressure per degree of pitch
$\Phi(\xi_i)$ = Eq. (11)
χ_i = $x(\eta_i)/x - (\xi_i/x)t(\eta_i)/t$
$\Psi(\xi_i)$ = Eq. (20)
balanced operation = jet condition for which there is no net mass flow into or out of the cushion
compartmentation = division of the cushion by introducing stability jets along the base of the craft

---

Received March 22, 1965; revision received August 5, 1965. The authors wish to extend their thanks to Vickers-Armstrongs (South Marston) Ltd., for permission to publish this report, to N. W. Lewis and M. J. Bennison for assistance with the development of the theory, and to Connie Mantych for typing the original manuscript.

* Senior Aerodynamicists; now Research Materials Engineer, Air Force Materials Laboratory, Wright-Patterson Air Force Base, Ohio.

† Senior Aerodynamicist; now Teacher, Park Grammar School, Swindon, Wiltshire, England.

cushion = volume of relatively high-pressure air supporting the craft and generated by the peripheral jets
hoverheight = vertical distance from nozzle exit to ground
longitudinal = the major axis of the craft
overfeed = jet condition where air enters the cushion by virtue of the peripheral jet splitting
St. George = arrangement whereby the stability jets lie along the major axis and normal to the major axis of the craft (see Fig. 1)
St. Andrew = arrangement whereby the stability jets lie along the diagonals of the craft base
transverse = normal to major axis of craft
underfeed = jet condition whereby air leaves the cushion by flowing under the peripheral jet
underfeed height = vertical distance by which peripheral jet is raised from the ground by air flowing under it

Introduction

It is well known[1–5] that GEM supported only by a jet around the periphery will be either unstable, or only slightly stable, in pitch and roll displacement. In order to ensure adequate stability, it has been the practice in the United Kingdom in recent years to introduce cushion compartmentation in the form of additional, vertically discharging, jets in the base of the craft. The stability jets are capable of sustaining a pressure differential, and it is found that, if the craft is now tilted, the static pressure will rise in those compartments approaching the ground, whereas that in the opposite compartments will fall. This gives rise to a restoring couple. Experience has shown that the thickness of the stability jets must be about the same as that of the peripheral jets for the stability to be adequate. Other methods of stabilization have also been reported, as for instance in Ref. 6.

The problem of calculating the pitch or roll stiffness of a three-dimensional craft has given investigators some difficulty, although progress has been made in the two-dimensional case.[1,7,8] Difficulty has arisen also over the interpretation and reduction of the limited amount of experimental data available.

The present report describes a theoretical method of obtaining the stiffness of any peripheral jet GEM. Basically, the procedure adopted is to obtain expressions for the mass flows entering and leaving each compartment and then to use the condition of continuity of mass flow as the basis of an iteration procedure. The theory indicates a way in which experimental data can be reduced for any given craft shape. The agreement between theory and experiment, both for models and full scale craft with a St. George stability arrangement, is encouraging.

It was felt that no assessment of the effects of cushion vortices could be made without greatly complicating the analysis and obscuring the main features. However, some recent investigations of cushion vortices are of interest, and these are described in Refs. 9 and 10.

Theory of Pitch Stability

Consider any three-dimensional GEM with a peripheral jet represented by the curve $ABCDA$ of Fig. 1. Air flows through

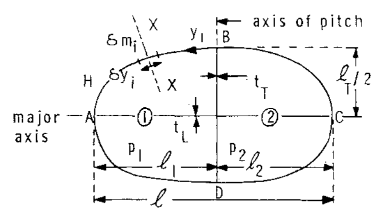

Fig. 1 Plan view of craft base.

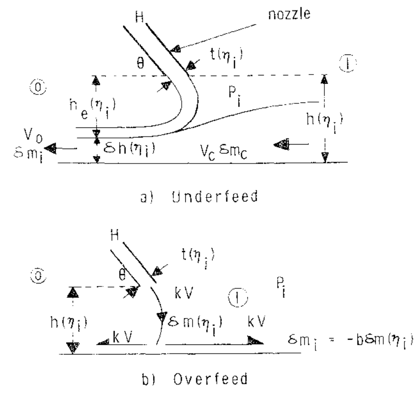

Fig. 2. Section of peripheral jet (XX in Fig. 1).

this nozzle, inclined at some angle θ to the outward horizontal as in Fig. 2, and maintains the cushion pressure under the craft. In the St. George stability arrangement, compartmentation is provided by means of additional vertically discharging jets represented by the lines BD and AC in Fig. 1. The four compartments so produced can all be at different static pressures but, in the case of pitch displacement alone, the two front compartments are at single pressure p_1 and are lumped into a single compartment ①, in the present analysis; a similar convention is adopted for the rear compartments. Air for the jets must be provided by means of a suitable fan engine combination. This will supply a total head rise δH across the fan(s), but losses in the ducting will ensure that the total head of the air, by the time it emerges from the nozzles, will be some lower figure H. It is assumed that the losses are uniform so that H is a constant everywhere. This will be approximately true for well made ducts. In the present stability analysis H need not be known but would have to be known for a more general performance calculation as a function of the total mass flow through the system. A detailed knowledge of engines, fans, and losses in the system then would be required.

If the craft shown in Fig. 1 is tilted now nose down, the static pressure p_1 in the front compartment will rise, whereas the pressure p_2 in the rear compartment will fall. The pressure differential therefore causes a couple that opposes the displacement. It is the purpose of this investigation to calculate the restoring couple and to express it in a nondimensional form for comparison with experiment.

It is assumed that the pressure p_i in the ith compartment ($i = 1, 2$) is constant everywhere, and that vortices in each compartment have a negligible effect. This implies that p_i/H must be constant in each compartment. It is observed in Appendix A that, for a balanced jet, p_i/H depends significantly on a quantity x alone, where $x = h/t(1 + \cos\theta)$, h is the hoverheight, t is the jet thickness, and θ is the angle between the jet and the horizontal. For the unbalanced jet therefore we may define a quantity ξ_i such that ξ_i is the effective value of x in the ith compartment, i.e. that value of x for which a balanced jet would have the same value of p_i/H. On this basis, the equations of Appendix A give

$$f_i = p_i/H = f(\xi_i) \tag{1}$$

$$\delta m(\eta_i)/t(\eta_i)S_i\delta\eta_i(\rho H)^{1/2} = g(\xi_i) \tag{2}$$

where $\xi_i = h_e(\eta_i)/t(\eta_i)(1 + \cos\theta)$ at any station η_i of the periphery. The quantity $h_e(\eta_i)$ is the effective height of the jet at station η_i and is yet to be determined; $\delta m(\eta_i)$ is the mass flow out of the elementary peripheral nozzle of length δy_i at station η_i. If we let m_{pi} be the total mass flow out of the peripheral nozzle in the ith compartment and integrate Eq. (2) with respect to η_i, we obtain

$$\frac{m_{pi}}{(H)^{1/2}} = (\rho)^{1/2}tS_ig(\xi_i)\int_0^1 \frac{t(\eta_i)}{t}\,d\eta_i \tag{3}$$

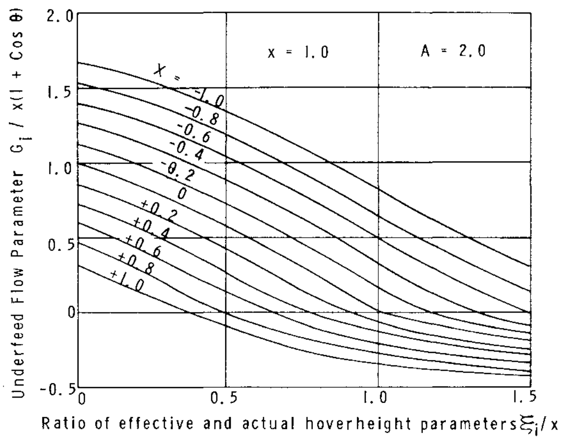

Fig. 3. Graphs of $G_i/x(1 + \cos\theta)$ against ξ_i/x.

where t is the jet thickness at any reference point, for example the point $\eta_i = 0$ (point B in Fig. 1).

Now, when the craft is tilted nose down, part of the front peripheral jet will approach the ground, whereas the rear of the craft will be raised. This means that, in effect, a large gap will appear under the rear peripheral jet, and this will have to be filled up by air from the front compartment. Some of this additional air, therefore, may have to be made up by part of the front peripheral jet operating in the splitting or overfeeding state. Two regimes of jet operation therefore will occur. We shall examine each of these in turn.

Analysis of Underfeeding Jet

Any air entering the ith compartment (for example, from stability jets and/or splitting parts of the peripheral jets) must leave the cushion by underfeeding at least part of the peripheral jet. Consider a section of nozzle of length δy_i at station η_i as in Fig. 2. It is assumed, as stated earlier, that vortices in the compartments will be ignored, so that the air will lose little of its momentum in crossing the cushion. Therefore, with comparatively little error, we may assume that

$$\delta m_c V_c = \mu \delta m_i V_s \tag{4}$$

where V_s is the velocity with which the crossflow air enters the cushion; V_s is taken to be close to the velocity of the air through the stability nozzles; μ is a factor describing the loss of momentum and will be close to unity; and δm_i is the mass flow under section δy_i of the peripheral jet at station η_i. Now we apply Newton's Second Law to the flow from ① to ⓪ in Fig. 2, so that

$$P_i \delta h(\eta_i) \delta y_i = \delta m_i V_0 - \delta m_c V_c$$

$$p = \delta m_i (V_0 - \mu V_s) \tag{5}$$

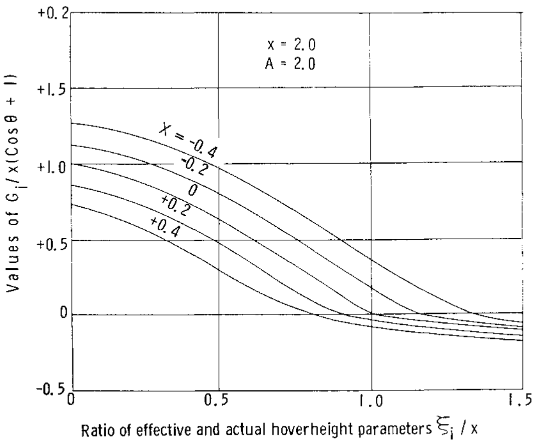

Fig. 4 Graphs of $G_i/x(1 + \cos\theta)$ against ξ_i/x.

using Eq. (4). In Eq. (5), the velocity V_0 is given by

$$V_0 = \delta m_i / \rho \delta y_i \delta h(\eta_i) \tag{6}$$

where $\delta h(\eta_i)$ is the underfeed height, i.e. the amount by which the peripheral jet is raised from the ground by the underfeeding air. The velocity V_s is obtained by applying Bernoulli's equation to the flow through the stability nozzles. Therefore, approximately,

$$H = p_i + \tfrac{1}{2}\rho V_s^2 \qquad \therefore V_s = [2(H - p_i)/\rho]^{1/2} \tag{7}$$

Now we write $G_i = m_i/S_i t(\rho H)^{1/2}$, where m_i is the total amount of air leaving the ith compartment by way of the periphery in unit time. Then, clearly, $\delta G_i = \delta m_i / S_i t(\rho H)^{1/2}$. Putting Eq. (6) into Eq. (5) and using Eq. (7), we now have

$$p_i \delta h(\eta_i) S_i \delta \eta_i = \delta m_i [\delta m_i / \rho \delta y_i \delta h(\eta_i) - \mu (2/\rho)^{1/2} (H - p_i)^{1/2}]$$

$$\therefore p_i \delta h^2(\eta_i) S_i = (\delta m_i/\delta \eta_i)[(1/\rho S_i)(\delta m_i/\delta \eta_i) - \mu(2H/\rho)^{1/2}(1 - f_i)^{1/2} \delta h(\eta_i)] \tag{8}$$

Taking the limit as $\delta \eta_i \to 0$ and substituting for G_i, we then put Eq. (8) in the form

$$f(\xi_i)\frac{\delta h^2(\eta_i)}{t^2(\eta_i)} = \frac{t^2}{t^2(\eta_i)}\left[\frac{\partial G_i}{\partial \eta_i}\right]^2 - 2^{1/2}\mu[1 - f(\xi_i)]^{1/2}\frac{\delta h(\eta_i)}{t(\eta_i)}\frac{t}{t(\eta_i)}\frac{\partial G_i}{\partial \eta_i} \tag{9}$$

Equation (9) may be rearranged as an equation for $h(\eta_i)/t(\eta_i)$ and solved to give

$$\delta h(\eta_i)/t(\eta_i) = [t/t(\eta_i)\Phi(\xi_i)][\partial G_i/\partial \eta_i] \tag{10}$$

where

$$\Phi(\xi_i) = \frac{2^{1/2} f(\xi_i)}{[\mu^2 + (2 - \mu^2) f(\xi_i)]^{1/2} - \mu[1 - f(\xi_i)]^{1/2}} \tag{11}$$

The function $\Phi(\xi_i)$ is drawn out readily. The effect of μ is found to be comparatively small, and μ will be taken as unity in the calculations. It is seen also from Fig. 2 that

$$\xi_i(1 + \cos\theta) = h(\eta_i)/t(\eta_i) - \delta h(\eta_i)/t(\eta_i) \tag{12}$$

so that substituting Eq. (1) into Eq. (12) gives

$$\xi_i(1 + \cos\theta) = h(\eta_i)/t(\eta_i) - [t/t(\eta_i)\Phi(\xi_i)][\partial G_i/\partial \eta_i] \tag{13}$$

$$\therefore \partial G_i/\partial \eta_i = \Phi(\xi_i)[h(\eta_i)/t - \xi_i t(\eta_i)(1 + \cos\theta)/t]$$

$$\partial G_i/\partial \eta_i = x(1 + \cos\theta)\Phi(\xi_i)[x(\eta_i)/x - \xi_i t(\eta_i)/xt] \tag{14}$$

where $x = h/t(1 + \cos\theta)$, $x(\eta_i) = h(\eta_i)/t(1 + \cos\theta)$, and h is the hoverheight at station $\eta_i = 0$. Equation (14) may now be integrated with respect to η_i to give

$$\frac{G_{i+}}{x(1 + \cos\theta)} = \Phi(\xi_i)\int \chi_i d\eta_i \tag{15}$$

where the integral gives only the positive part of G_i and must be taken over only the positive values of χ_i where

$$\chi_i = [x(\eta_i)/x] - (\xi_i/x)[t(\eta_i)/t]$$

The procedure adopted previously is not the only way of calculating $\Phi(\xi_i)$. If, for example, Bernoulli's theorem had been applied to the flow between points ① and ⓪ in Fig. 2, instead of Newton's Second Law, and all the previous assumptions had been retained apart from the additional neglect of loss of total head in the crossflow, then the value of $\Phi(\xi_i)$ would have been $2^{1/2}$ for all ξ_i. This is not markedly different from the values given by Eq. (11) for μ close to unity. No experimental data are known to be available to compare with, unfortunately. However, examination of the graphs of $G_i/x(1 + \cos\theta)$ against ξ_i/x in Figs. 3 and 4 shows that there is little likelihood of these differences in $\Phi(\xi_i)$ being reflected as measurable changes in the theoretical curve of pitch stiffness against x to be obtained presently.

Analysis of Overfeeding Jet

Equation (15) represents the fraction of G_i that leaves the cushion by underfeeding part of the peripheral jet. The net flow out of the cushion may be less than G_{i+}, however, since a certain amount of air may enter the compartments because of the splitting of part of the peripheral jet. The equation of a splitting jet, derived in Appendix B and given by Eq. (B4), may be written

$$b = \frac{1}{2}(1 + \cos\theta)\left[1 - \frac{t}{t(\eta_i)}\,\frac{x(\eta_i)}{\xi_i}\right] \tag{16}$$

where ξ_i is defined in Eq. (1). The net inflow δm_i therefore is given by

$$\delta m_i = -b\delta m(\eta_i)$$

$$\delta m_i = -\frac{1}{2}(1 + \cos\theta)\left[1 - \frac{t}{t(\eta_i)}\,\frac{x(\eta_i)}{\xi_i}\right] \times t(\eta_i)S_i\delta\eta_i(\rho H)^{1/2}g(\xi_i) \tag{17}$$

using Eqs. (2) and (16). Equation (17) may be rearranged and the limit taken as $\delta\eta_i \to 0$ to give

$$\frac{\partial G_i}{\partial \eta_i} = -\frac{g(\xi_i)}{2\xi_i}(1 + \cos\theta)\left[\frac{\xi_i}{x}\,\frac{t(\eta_i)}{t} - \frac{x(\eta_i)}{x}\right] \tag{18}$$

Equation (18) may be integrated with respect to η_i to give the negative part of G_i:

$$G_{i-}/x(1 + \cos\theta) = \psi(\xi_i)\int\chi_i d\eta_i \tag{19}$$

where

$$\psi(\xi_i) = g(\xi_i)/2\xi_i \tag{20}$$

The integral in Eq. (19) is to be taken over only the negative values of χ_i. The algebraic sum of Eqs. (15) and (19) gives the net value of G_i, i.e.,

$$G_i/x(1 + \cos\theta) = I_+\Phi(\xi_i) + I_-\psi(\xi_i) \tag{21}$$

where I_+ and I_- are the positive and negative parts, respectively, of the integral

$$I = \int_0^1 \chi_i\, d\eta_i \tag{22}$$

For any particular craft geometry, I_+ and I_- may be evaluated numerically as functions of x and ξ_i. Values of I_+ and I_- are given in Fig. 5 for a rectangular geometry of aspect ratio $A = 2$. It will be noted that $I_+(\xi_i/x, +X) = -I_-(2 - \xi_i/x, -X)$, and that $I_-(\xi_i/x, +X) = -I_+(2 - \xi_i/x, -X)$. These simple relationships may easily be proved geometrically by plotting χ_i against η_i. Figure 5 illustrates the point. It remains to consider the equations of the stability jets. Many types of stability arrangement may be studied, but only the St. George configuration will be dealt with in the present analysis.

St. George Stability Arrangement

Consider first the transverse stability jet. Let m_{s3} be the mass flow through the transverse stability nozzle, and let m_{s31} and m_{s32} be the mass flows in the branches of this jet entering the front and rear compartments, respectively. For the nose-down case $p_1 > p_2$, the equations of Appendix A give

$$(f_1 - f_2)/(1 - f_2) = f(\xi) \tag{23}$$

$$m_{s3}/H^{1/2} = l_T t_T(\rho)^{1/2}g(\xi)(1 - f_2)^{1/2} \tag{24}$$

where ξ is the effective value of x for this particular jet. Note that p_2 takes the place of atmospheric pressure as datum in this case. If $\xi > h/t_T$, the transverse stability jet will be splitting and the equations of Appendix B will be applicable, i.e.,

$$m_{s31}/m_{s3} = \tfrac{1}{2}(1 - h/\xi t_T) \tag{25}$$

since the angle of the jet is 90°. If, on the other hand, $\xi < h/t_T$, the transverse stability jet will operate in the under-

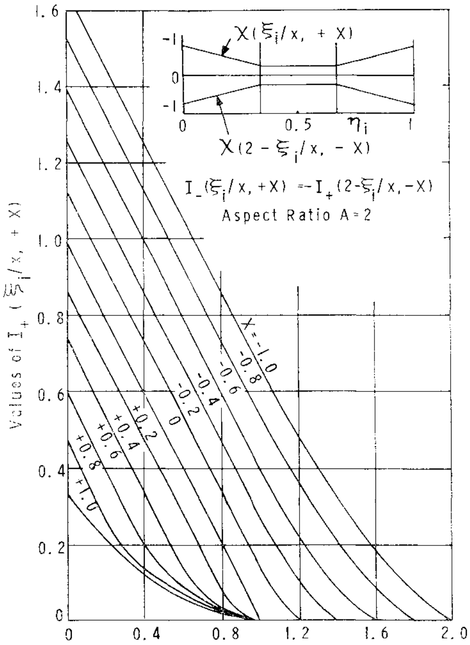

Fig. 5 Graphs of I_+ against ξ_i/x.

feeding state, and the underfeed height by which it is raised from the ground is given by

$$\delta h/t_T = h/t_T - \xi \tag{26}$$

as illustrated in Fig. 6.

If $-m_{s31}$ is the mass flow under the transverse stability jet entering the compartment ① (the negative sign indicates that it is actually leaving), Newton's Second Law may be applied to the flow from ① to ② in Fig. 6 to give

$$(p_1 - p_2)\delta h l_T = -m_{s31}(V_2 - V_1) \tag{27}$$

where V_1 and V_2 are the average velocities of the flow m_{s31} before and after underfeed, respectively. Therefore $V_1 = -m_{s31}/l_T\rho h$ and $V_2 = -m_{s31}/l_T\rho\delta h$. Putting these expressions for V_1 and V_2 into Eq. (27) gives an equation for m_{s31} which may be solved to give

$$\frac{m_{s31}}{H^{1/2}} = -\rho^{1/2}l_T t\left[\frac{(f_1 - f_2)}{(t/\delta h)(t/\delta h - t/h)}\right]^{1/2} \tag{28}$$

Needless to say, this equation is approximate, and it would have been equally acceptable to have applied Bernoulli's equation to the flow between regions ① and ② in Fig. 6. This would have led to a different expression for $m_{s31}/H^{1/2}$, but it is found that there is no great difference between the two results. Moreover, since the stability jets operate in the underfeeding state only when the craft incidence is a large fraction (X large) of the maximum possible incidence at a given hoverheight, this difference will not affect the calculations over the initial incidence range (X small).

For the longitudinal stability jets, when the craft is inclined in pitch only, there will be no pressure differential, and so the appropriate value of ξ is infinity; $g(\xi) = 2^{1/2}$ for $\xi = \infty$. The mass flows m_{s1} and m_{s2} through the front and rear parts, respectively, of the longitudinal stability jets, therefore are given by

$$m_{si}/H^{1/2} = l_i t_L(2\rho)^{1/2}(1 - f_i)^{1/2} \tag{29}$$

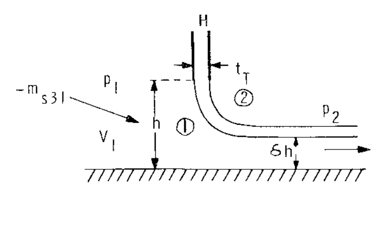

Fig. 6 Section of transverse stability jet.

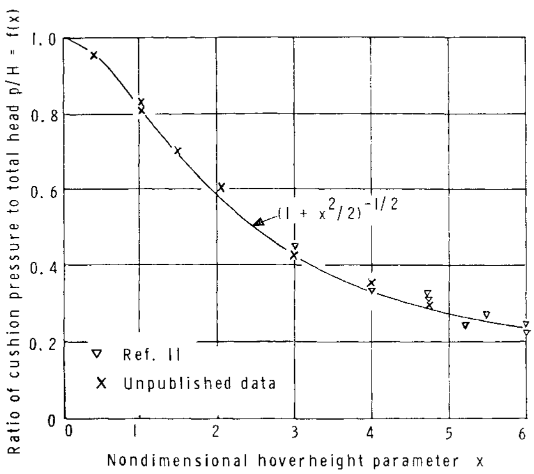

Fig. 7 Values of p/H for balanced jet.

Evaluation of I_+ and I_-

For a rectangular craft with symmetry about both the transverse and longitudinal stability jets, the incidence is measured in terms of a quantity X where the hoverheight at the low end of the craft is $h(1 - X)$ and that at the high end is $h(1 + X)$; X can take any value in the range $-1 < X < 1$, and intervals of 0.2 have been found to be adequate. The kernel of the integral in Eq. (22) can be plotted as a function of η_i for given $t(\eta_i)/t$, ξ_i/x, and X. Then I_+ and I_- are simply the positive and negative areas, respectively, under the curves and are evaluated easily. For the rectangular planform, the calculations are particularly simple, since the graphs of χ_i against η_i are made up of straight segments. The results of the calculations are given in Fig. 5. Now $G_i/x(1 + \cos\theta)$ can be calculated as a function of x and ξ_i. The procedure adopted was to choose values of x and ξ_i. Then ξ_i/x was calculated and I_+, I_- read off for the appropriate X. Substitution in Eq. (21) then gave the required result. Some graphs of $G_i/x(1 + \cos\theta)$ are shown in Figs. 3 and 4 for $x = 1, 2$, respectively. Slight differences arise for different x but they are sufficiently small for interpolation to be simple.

Method of Solution for St. George Configuration

The iteration procedure described following is the only method that has been found to converge with any degree of consistency. Initial values of ξ_1 and ξ_2 are guessed, and f_1, f_2 are obtained from Eq. (1) and Fig. 7. The ratio m_{s31}/m_{s3} is then using calculated Eqs. (23–25); $m_{s1}/H^{1/2}$ is obtained from Eq. (29), and G_i is then obtained readily since

$$G_1 = (m_{s31} + m_{s1})/S_1t(\rho H)^{1/2} \tag{30}$$

and similarly for G_2. For given x and θ, therefore, $G_i/x(1 + \cos\theta)$ can be calculated. For a chosen value of X, new values of ξ_1 and ξ_2 then are read off the graphs of $G_i/x(1 + \cos\theta)$ against ξ_i/x. The process is repeated until convergence occurs. It is not particularly straightforward since two variables are involved and some ingenuity is needed.

When the process has converged, f_1 and f_2 will be known. The nose-up moment about the pitch axis (line BD in Fig. 1) then is given by

$$\begin{aligned} M &= p_1(l_Tl/2)(l/4) - p_2(l_Tl/2)(l/4) \\ &= l_Tl^2H(f_1 - f_2)/8 \end{aligned} \tag{31}$$

if momentum lift due to the direct thrust of the jets is neglected. Since the mass flow rate through the nozzles also is readily calculated in terms of ξ_1 and ξ_2, the contribution of the momentum lift to M is obtained readily and usually is found to be small. Similarly, the lift on the base of the craft is

$$\begin{aligned} L &= p_1(l_Tl/2) + p_2(l_Tl/2) \\ &= l_TlH(f_1 + f_2)/2 \end{aligned} \tag{32}$$

The percentage shift N of the center of pressure, based on the length l, therefore is given by

$$N = \text{Moment} \times 100\%/\text{Lift} \times l = [25(f_1 - f_2)]/(f_1 + f_2) \tag{33}$$

using Eqs. (31) and (32). Now this value of N corresponds to a given x and X. The calculations therefore are repeated for a number of values of x and X, and it is found that, for $X < 0.4$ or so, the graphs of N against X are linear. The maximum pitch displacement for a rectangular craft is $\alpha_{\max} = 2h/l$ rad, where h is the hoverheight at station $\eta_i = 0$. The actual incidence for given X is therefore

$$\alpha = X\alpha_{\max} = 360\ X\ h/\pi l \text{ deg} \tag{34}$$

In view of the fact that the graphs of N against X are linear for small X, the pitch stiffness expressed as a percentage shift of the center of pressure (based on the length l) per degree of incidence change is

$$\begin{aligned} \sigma &= N/\alpha = \pi N/360\ X\ (h/l) \\ \sigma h/l &= \pi N/360\ X \end{aligned} \tag{35}$$

where N/X is a constant. The theory therefore indicates that $\sigma h/l$ will be a function of x alone for a given geometry. It is found that the dependence on the jet angle θ is small provided that $\theta < 60°$ or so. If we plot $\sigma h/l$ against x, therefore, the same results should be obtained for all sizes of craft with similar geometry. Figure 8 shows some theoretical and experimental results for a rectangular craft of aspect ratio $A = 2$ in pitch. The experimental points relate to craft that differ in many ways from this aspect ratio and the rectangular planform. In view of this, the agreement between theory and experiment is encouraging. Figure 8 also shows the results for the same craft in roll, for which the aspect ratio is effectively $A = \frac{1}{2}$. It is seen that the effect of aspect ratio, like that of the jet angle θ, is small.

Conclusions

A theory has been developed which relates the macroscopic behavior of a three-dimensional peripheral jet GEM in pitch and roll to the characteristics of the peripheral and stability jets, which may be obtained from two-dimensional experiments. The available data do not contradict the theory, but the scatter is so great that further data are clearly required. The development of the theory also has brought to light a serious gap in our understanding of the quantitative behavior of two-dimensional jets operating in the unbalanced state. A framework has been established which should assist in the interpretation of any experimental data that may become available.

Appendix A: The Balanced Jet

The simplest form of jet is that issuing from a double-walled, parallel sided (or very slightly convergent) nozzle. In the balanced state, there is no net flow into, or out of, the cushion of relatively high-pressure air maintained by the jet. The value of p/H, where p is the cushion static pressure referred to atmospheric pressure as datum, and H is the total head of the air issuing from the nozzle referred to the same datum, is found to depend primarily on $x = h/t(1 + \cos\theta)$, where h is the hoverheight, t the jet thickness, and θ is the nozzle angle relative to the horizontal on the low-pressure side of the jet[1,2,11–13]; p/H also depends very slightly on the size and geometry of the cushion by virtue of the effects of entrainment and cushion vorticity, but these effects are not isolated easily. They are, however, usually small. The other parameter on which p/H depends is the Reynolds number Vt/ν, where V is the nozzle velocity of the jet and ν the kinematic viscosity of the fluid. For values in excess of 20,000 or so, based on a mean velocity, the jet Reynolds number is found in practice to have little effect. The ratios $m/St(\rho H)^{1/2}$ and $m/St(\rho p)^{1/2}$, where m is the mass flow through the nozzle and S the nozzle length, are nondimensional also and depend primarily on x and secondarily on entrainment and jet Reynolds number. Graphs of p/H and $m/St(\rho p)^{1/2}$ are drawn in Figs. 7 and 9, respectively, the experimental points being obtained from a variety of sources and for a wide range of jet sizes. The graph of $m/St(\rho H)^{1/2}$ is not presented since it is shown readily that

$$g(x) = \gamma(x)[f(x)]^{1/2} \tag{A1}$$

where $f(x) = p/H$, $\gamma(x) = m/St(\rho p)^{1/2}$, and $g(x) = m/St(\rho H)^{1/2}$. It should be noted that both p and H refer to atmospheric pressure as datum in this instance. It is also of interest to note that, although no theoretical justification is known, $f(x)$ and $\gamma(x)$ can be represented with good accuracy by the following very simple empirical relationships:

$$f(x) = 1/(1 + \tfrac{1}{2}x^2)^{1/2} \tag{A2}$$

$$\gamma(x) = (5x/4)^{1/2} \tag{A3}$$

Appendix B: The Splitting Jet

If a jet is stronger than is necessary to support a cushion pressure p at hoverheight h, its curvature will be smaller than for a balanced jet at the same hoverheight, and the jet must split as in Fig. 2. The fraction b of the mass flow m from the nozzle per unit time, which enters the high-pressure side, is to be determined. The simplest theory available is the so-called momentum theory. Although the velocity in the nozzle is $V(=m/\rho St)$, where t is the jet thickness and S the nozzle length, the velocity in the jet outside the nozzle will be lower. The losses involved in the splitting process are assumed to reduce the jet velocity everywhere by some factor k, as in Fig. 2. Newton's Second Law is then applied to the flows in the splitting process so that

$$\begin{aligned} pSh &= (1 - b)mkV - bmkV + mkV\cos\theta \\ &= mkV(1 + \cos\theta - 2b) \end{aligned} \tag{B1}$$

But $p/H = f(\xi)$ where ξ is the effective value of x i.e., the value of x for the balanced jet which gives the same value of p/H. We note that $\xi > h/t(1 + \cos\theta)$. It is further assumed that the mass flow per unit time through the nozzle depends on ξ alone so that $m/St(\rho p)^{1/2} = \gamma(\xi)$ and does not depend in any way on $x = h/t(1 + \cos\theta)$. Equation (B1) may be rewritten therefore in the form

$$h/t = \gamma^2(\xi)k(1 + \cos\theta - 2b) \tag{B2}$$

If k is assumed to be unity, we recover the simplest form of the momentum theory but, when $b = 0$, this implies that $\xi/\gamma^2(\xi) = 1$ because the jet is then balanced and $\xi \equiv x$. However, $\xi/\gamma^2(\xi) \neq 1$, as may readily be shown.

If, on the other hand, k is assumed to be a function of ξ alone, the substitution $b = 0$ when $\xi = x$ in Eq. (B2) leads to the simple result

$$k = k(\xi) = \xi/\gamma^2(\xi) \tag{B3}$$

Substitution of Eq. (B3) back into (B2) then gives

$$b = \tfrac{1}{2}(1 + \cos\theta)(1 - x/\xi) \tag{B4}$$

applicable for $\xi \geqslant x$. It is again true, unfortunately, that no experimental data seem to be available for comparison with Eq. (B3) and (B4). However, Eq. (B4) is seen to give $b = 0$ for $x = \xi$ as it should, and gives $b = \frac{1}{2}(1 + \cos\theta)$ for $\xi = \infty$, i.e., $p = 0$. This is the case of a jet discharging directly to atmospheric pressure and striking a plane wall at an angle θ to the wall. In this case also, Eq. (B4) seems to give a satisfactory result. For example, $\theta = 90°$ for $b = \frac{1}{2}$, and $\theta = 0$ for $b = 1$. Until experimental data are available, it will be necessary to find some theoretical relationship between b, ξ, θ, and x. Equation (B4) represents the simplest known relation.

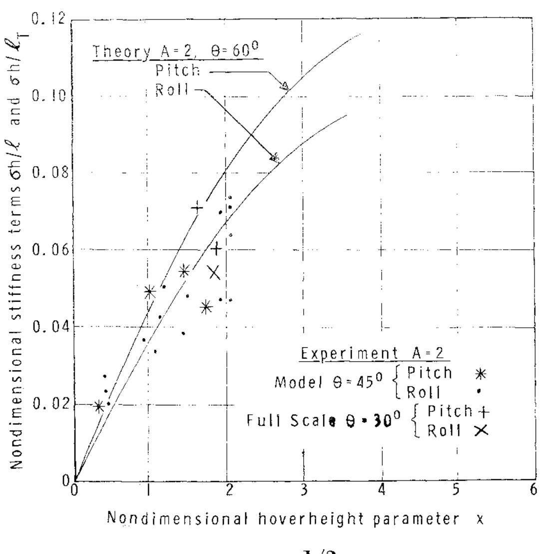

Fig. 8 Values of $m/St(\rho p)^{1/2}$ for balanced jet.

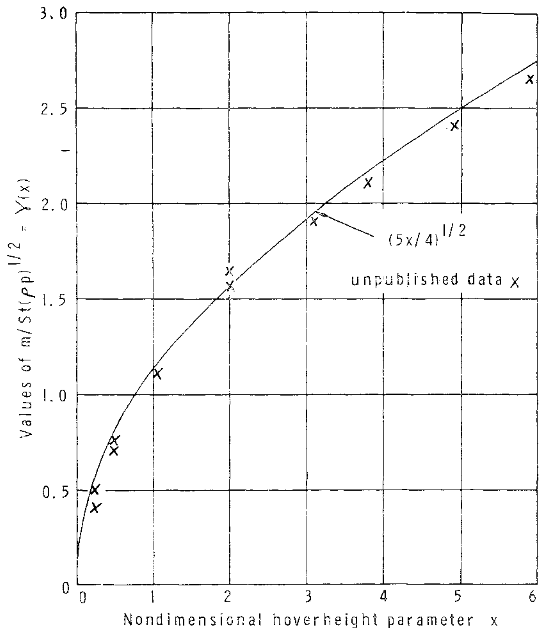

Fig. 9 Comparison between theoretical and experimental stiffness in pitch and roll.

References

[1] Eames, M. C., "Fundamentals of the stability and control of peripheral jet vehicles," Pneumodynamics Corp. Report, Bethesda, Md. (1960).

[2] Stanton-Jones, R., "The development of the Saunders-Roe hovercraft SRN-1," Aero. Research Council Rept. 21 491 (October 1959).

[3] Carmichael, B. H., "Hovering static stability and performance experiments on three-dimensional annular jet models," Transportation Research and Engineering Command, Fort Eustis, Va., Rept. 62-36 (1962).

[4] Dau, K., "Characteristics of a rectangular wing with a peripheral jet in ground effect: Part 1," Institute of Aerophysics, Univ. of Toronto, Toronto, Ontario, Canada, Note 56 (September 1961).

[5] Webb, W. B., "Annular jet stability analyses in hovering," Bell Helicopter Co. Rept. 8034-099-001 (September 1960).

[6] Liiva, J., "Gyrostabilisation of an elliptic wing with peripheral jet hovering in ground effect," Institute of Aerophysics, Univ. of Toronto, Toronto, Ontairo, Canada, Note 60 (August 1962).

[7] Webster, W. C., "The static stability of ground effect machines—thin jet theory," Hydronautics Co., Rockville, Md., Rept. 011-1 (December 1960).

[8] Lin, J. D., "The static stability of ground effect machines—thick jet theory," Hydronautics Co., Rockville, Md., Rept. 011-2 (June 1961).

[9] Scott, W. J., "Asymmetry of annular jet flow in ground proximity," Institute of Aerophysics, Univ. of Toronto, Toronto, Ontairo, Canada, Note 61 (May 1962).

[10] Magnus, R. J., "Use of vortices in the calculation of bottom pressures of annular jet ground effect machines," Convair Report (March 1961).

[11] Yen, B., "Patterns of flow under a two-dimensional GEM," Iowa Institute of Hydronautics, Research Report (January 1962).

[12] Chaplin, H. R., "Ground effect machine research and development in the United States," David Taylor Model Basin Rept. 944 (December 1960).

[13] Poisson-Quinton, P. and Bevert, A., "The principle and applications of ground effect vehicles," Bull. Assoc. Tech. Maritime Aeronaut. 60, 61–89 (1960).

MARCH-APRIL 1966 J. AIRCRAFT VOL. 3, NO. 2

Strength Margins for Combined Random Stresses

J. R. Fuller*
The Boeing Company, Seattle, Wash.

Statistical mechanics procedures are widely used in the aerospace industry to analyze the effects of random loading on flight vehicles. Although existing procedures give the structures analyst considerable knowledge of the loads to which various parts of the vehicle are subjected, they do not provide a usable procedure for evaluating the structural strength of an element for combined random stresses. A procedure is derived herein, which permits a determination of the number of times per unit time that various strength margin levels are exceeded for combined random stresses.

Nomenclature

x, ξ = shear stress, psi
y, f = axial stress, psi
x_0, ξ_0, y_0, f_0 = steady stress values, shear and axial stress, respectively, psi
F_ξ = allowable shear stress, psi
F_t, F_c = allowable axial stress, psi
$\mathbf{z}$ = stress vector, $x\mathbf{i} + y\mathbf{j}$
$\dot{\mathbf{z}}$ = stress velocity vector, $\alpha\mathbf{i} + \beta\mathbf{j}$
$\sigma_x, \sigma_y, \sigma_\alpha, \sigma_\beta$ = root mean square values (standard deviations) for x, y, α, and β, respectively
$\Phi_x(\omega), \Phi_y(\omega)$ = power spectral density functions for random process $x(t)$ and $y(t)$, respectively
$\Phi_{xy}(\omega)$ = cross power spectral density function for $x(t)$ and $y(t)$
ω = circular frequency, rad/sec
ρ = correlation coefficient for $x(t)$ and $y(t)$
α, β = time rate of change of x and y, respectively
$p(x), p(y)$ = probability densities of x and y
$p(x, y)$ = joint probability density of x and y
$f(x, \alpha, y, \beta)$ = probability density of x, α, y, β
MS = margin of safety
$P(MS < 0)$ = probability that MS is less than zero, or percent time that MS is less than zero
$P(MS \geqslant 0)$ = probability that MS is greater than or equal to zero
C = a curve on the xy plane
$\mathbf{N}$ = unit vector normal on C
$[\ ]$ = column matrix
$\lfloor\ \rfloor$ = row matrix
N_c = crossings of an arbitrary curve/sec or /ft traveled
σ_w = root mean square gust velocity, fps
$f(\sigma_w)$ = probability density distribution of σ_w
V = velocity, fps
$\bar{G}$ = expected exceedances of limit design strength/hr
$\bar{A}$ = root mean square stress response for σ_w of unity, psi/fps
N_0 = number of times/unit time or distance that a time-history crosses its mean value with positive or negative slope

Received October 15, 1964; revision received October 18, 1965.

* Supervisor, Product Development, Structures Research Group, Structures Staff.

Introduction

THE strengths of various structural elements in aircraft and aerospace vehicles are usually defined in terms of a stress interaction function or interaction diagram such as that shown in Fig. 1. This type of diagram shows the various combinations of stresses which would cause the structural element to fail. Any combination of stresses within the envelope is allowable.

When a flight vehicle is subjected to random loading, such as continuous atmospheric turbulence, buffeting, a turbulent boundary layer, or engine noise, random stress components are generated in the various structural elements. It is important for the structures engineer to know the expected number of years, hours, or minutes that the structural element can sustain the combined random stresses before the strength is exceeded.

Development of the Procedure

Joint Probability Approach

For purposes of illustration, let us consider two stress components, axial stress and shear stress, on a segment of a stiffened skin panel, as shown in Fig. 1. Further, let us assume that each stress time-history is statistically stationary and has a Gaussian probability distribution when sampled at equal increments of time. If the time-histories were statistically independent, that is, if there were no correlation between them, their joint probability density function would